



## Article

# Thermal Storage of Nitrate Salts as Phase Change Materials (PCMs)

Marco A. Orozco <sup>1</sup>, Karen Acurio <sup>2</sup>, Francis Vásquez-Aza <sup>1</sup> , Javier Martínez-Gómez <sup>1,2,3,\*</sup>   
and Andres Chico-Proano <sup>4</sup>

- <sup>1</sup> Instituto de Investigación Geológico y Energético (IIGE), Quito EC170518, Ecuador; marco.orozco@geoenergia.gob.ec (M.A.O.); francisvasquezaza@gmail.com (F.V.-A.)  
<sup>2</sup> Campus Miguel de Cervantes, Universidad Internacional SEK (UISEK) Ecuador, Calle Alberto Einstein s/n y 5ta. Transversal, Quito EC170134, Ecuador; karen.acurioc@gmail.com  
<sup>3</sup> Departamento de Teoría de la Señal y Comunicación, Área de Ingeniería Mecánica, Escuela Politécnica, Universidad de Alcalá (UAH), 28805 Alcalá de Henares, Madrid, Spain  
<sup>4</sup> Departamento de Ingeniería Química, Escuela Politécnica Nacional, Ladrón de Guevara E11-253, Quito EC170525, Ecuador; andres.chico@epn.edu.ec  
\* Correspondence: javiermtnezg@gmail.com

**Abstract:** This study presents the energy storage potential of nitrate salts for specific applications in energy systems that use renewable resources. For this, the thermal, chemical, and morphological characterization of 11 samples of nitrate salts as phase change materials (PCM) was conducted. Specifically, sodium nitrate (NaNO<sub>3</sub>), sodium nitrite (NaNO<sub>2</sub>), and potassium nitrate (KNO<sub>3</sub>) were considered as base materials; and various binary and ternary mixtures were evaluated. For the evaluation of the materials, differential Fourier transform infrared spectroscopy (FTIR), scanning calorimetry (DSC), thermogravimetric analysis (TGA), and scanning electron microscopy (SEM) to identify the temperature and enthalpy of phase change, thermal stability, microstructure, and the identification of functional groups were applied. Among the relevant results, sodium nitrite presented the highest phase change enthalpy of 220.7 J/g, and the mixture of 50% NaNO<sub>3</sub> and 50% NaNO<sub>2</sub> presented an enthalpy of 185.6 J/g with a phase change start and end temperature of 228.4 and 238.6 °C, respectively. This result indicates that sodium nitrite mixtures allow the thermal storage capacity of PCMs to increase. In conclusion, these materials are suitable for medium and high-temperature thermal energy storage systems due to their thermal and chemical stability, and high thermal storage capacity.

**Keywords:** inorganic PCMs; thermal storage; nitrate salt mixtures



**Citation:** Orozco, M.A.; Acurio, K.; Vásquez-Aza, F.; Martínez-Gómez, J.; Chico-Proano, A. Thermal Storage of Nitrate Salts as Phase Change Materials (PCMs). *Materials* **2021**, *14*, 7223. <https://doi.org/10.3390/ma14237223>

Academic Editors: Francisco de Paula Montero Chacón and Juan Carlos Serrano-Ruiz

Received: 1 July 2021

Accepted: 5 August 2021

Published: 26 November 2021

**Publisher's Note:** MDPI stays neutral with regard to jurisdictional claims in published maps and institutional affiliations.



**Copyright:** © 2021 by the authors. Licensee MDPI, Basel, Switzerland. This article is an open access article distributed under the terms and conditions of the Creative Commons Attribution (CC BY) license (<https://creativecommons.org/licenses/by/4.0/>).

## 1. Introduction

Efficient energy storage systems have emerged because of the interest in reducing the greenhouse gas (GHG) emissions caused by the increasing energy demand [1]. Consequently, it is essential to boost the current alternatives to optimize the use of available energy resources and minimize the environmental impact caused by the usage of fossil fuels. In this sense, the improvement of efficient energy storage systems represents a crucial option to accomplish these objectives [2]. Furthermore, it is well known that renewable sources of energy are intermittent. That is why it is crucial to ensure and provide stability by implementing energy storage systems [3].

Thermal energy storage (TES) systems can store energy generated in an environment and released it when required [2]. Heat storage can be achieved using sensible heat (SHS), latent heat (LHS), and thermochemical (TQS) storage [1]. Particularly, LHS presents superior characteristics for heat storage over the other ones because of its high latent heat and consistent phase change temperatures [4]. Correspondingly, the volume of the system is less affected by using latent heat storage systems over sensible heat systems due to

their higher density and specific heat [5]. In this sense, LHS requires less volume for its function compared with SHS and TQS. Accordingly, phase change materials (PCM) present characteristics that make them an advantageous option for thermal energy storage.

In general, PCMs use the energy that a system absorbs or releases during its phase change (generally solid to liquid) and then dispose of that energy when it is needed [6,7]. Thermal storage by using PCMs is an opportunity to accomplish energy security with efficiency by taking care of the environment [8]. In addition, PCMs have characteristics such as high energy storage density and an isothermal process during the phase change that allow a small footprint, make them more attractive as TES systems, and have a competitive cost [9]. According to the operating temperature, there are different types of PCMs such as those with low, medium, and high latent heat thermal energy storage. In this way, the operating temperature is defined by the melting temperature of the PCM [10]. Moreover, for a PCM, it is important to establish its storage capacity by measuring the value of the heat of fusion. Additionally, other properties such as high enthalpy of fusion, the temperature of phase change within the operating range of the system, chemical and thermal stability, non-toxicity, non-flammability, availability, and affordability are imperative to select a PCM for a specific use [1]. Furthermore, phase change memory (PCM) devices are enabled by amorphization, and crystallization-induced changes in the devices' electrical resistances [11].

On the other hand, it is possible to identify three types of PCMs based on their source: organic (fatty acids, paraffins, alkanes), inorganic (metals, alloys, salts, salt hydrates), and eutectics (organic and inorganic, organic-inorganic mixtures) [12]. Indeed, inorganic PCMs present advantages such as high energy storage. Inorganic PCMs have a higher capacity to store energy, higher operating temperatures, higher thermal conductivity, and lower cost compared with organic PCMs [12]. Even though inorganic PCMs have the drawback of being corrosive to metals, encapsulation of the PCM can be used to prevent this problem [13,14]. For example, Xu et al., (2017), analyzed the use of diatomite as a shape stabilization material for sodium nitrate. It was determined that the composite material presented low corrosiveness, high energy density, and high thermal stability [15]. In the same way, expanded vermiculite was used to form a composite with sodium nitrate. Similarly, good stability and low corrosiveness were achieved [4]. Additionally, salt hydrates present a disadvantage that is undercooling [6]. In this sense, it is better to work with dehydrated salts.

Particularly, in inorganic salts, the most used anions are nitrates, nitrate/nitrite mixtures, carbonates, chlorides, and fluorides, and cations belonging to alkaline elements such as sodium or potassium [3]. In this sense, materials such as potassium nitrate ( $\text{KNO}_3$ ), sodium nitrate ( $\text{NaNO}_3$ ), and sodium nitrite ( $\text{NaNO}_2$ ) have melting points at suitable temperatures to be used in thermal storage applications, exceeding  $150^\circ\text{C}$ , such as solar thermal systems [5]. For example, a study by Bauer, T., determined, using DSC, the high enthalpy of fusion of  $\text{NaNO}_3$  ( $178\text{ kJ}\cdot\text{kg}^{-1}$ ) [16]. Kourkova L. et al. evaluated the enthalpy of fusion of  $\text{NaNO}_2$ . They found a temperature of fusion of  $164^\circ\text{C}$  and enthalpy of fusion corresponding to  $13.9\text{ kJ}\cdot\text{mol}^{-1}$  [17]. Additionally, it was determined the melting temperature ( $336^\circ\text{C}$ ) and the high enthalpy of fusion of  $\text{KNO}_3$  ( $116\text{ kJ}\cdot\text{kg}^{-1}$ ) by calorimetry [18].

Furthermore, studies have been developed to enhance heat transfer and energy storage applications with nano/microparticles suspended [19–24]. Some examples can be seen in the research of Ho et al., Forced convection heat transfer of Nano-Encapsulated Phase Change Material (NEPCM) suspension in a mini-channel heatsink [20], in which NEPCMs with particle sizes in the range of 250–350 nm were synthesized. The synthesized NEPCM-water suspension is employed as the working-fluid for heat removal from a microchannel heatsink. Further research that shows the effect of microencapsulation is that developed by Eisapour et al., Exergy and energy analysis of wavy tubes photovoltaic-thermal systems using microencapsulated PCM nano-slurry coolant fluid [21], in which a more efficient water-cooled photovoltaic-thermal system with wavy tubes was developed. Additionally, the consequences of coolant fluid including water, Ag/water nanofluid, microencapsulated

phase change material slurry, and a new type of cooling fluid called microencapsulated phase change material nano-slurry, were studied. Hajjar et al., in Time periodic natural convection heat transfer in a nano-encapsulated phase-change suspension [22], developed the natural convection of NEPCMs suspension in a cavity with a hot wall with a time-periodic temperature. In addition, the article of Talebizadehsardari et al., Consecutive charging and discharging of a PCM-based plate heat exchanger with zigzag configuration [23], studied the remarkable energy savings, isothermal nature of the operation and low costs, energy storage with a plate type heat exchanger with zigzag configuration.

In this way,  $\text{SiO}_2/\text{Al}_2\text{O}_3$  nanoparticles added to Solar Salt can increase the heat of fusion by 7.4% and the specific heat by 52.1% in the solid phase and 18.6% in the liquid phase [19]. Another study found that by adding 1.0 wt % of silica as nanofluid into Solar Salt, it is possible to increase the heat capacity by 26.7% [25]. Additionally, CuO-doped nitrate salts were studied, evidencing increased thermal conductivity, diffusivity, and stability [26]. Nevertheless, a negative effect has been determined with the use of nanoparticles into the salts for the abovementioned purpose due to a notable increase in the corrosiveness of the salts [27–32].

Moreover, binary and ternary combinations of these salts have shown improved properties. To illustrate, the work developed by Berg [6] presents the binary phase diagram between  $\text{NaNO}_2$  and  $\text{NaNO}_3$ . This study determined that the mixture is a e.

Eutectic system with a solid point at 230 °C between a range of 0.25 to 0.80 of  $\text{NaNO}_3$  molar fraction. Additionally, the combination of  $\text{NaNO}_3$  and  $\text{KNO}_3$  in percentages of 60 and 40, respectively, is a mixture known as “Solar Salt”, whose eutectic is around 54%  $\text{KNO}_3$  and 46%  $\text{NaNO}_3$  and its melting point is approximately 222 °C, its minimum operating temperature is 290 °C, and the maximum operating temperature is about 585 °C [7–12,16–18,27–70]. Previous studies indicate that the mixture of these two compounds, in the indicated proportions, presents advantages such as high energy density, high heat capacity, low cost (about 6.68 \$/kg), and suitable properties for their operation at high temperatures [7–12,16–18,27–72]. Additionally, according to [37] and [36], the maximum temperature or the limit of stability of the samples is normally defined as the temperature at which the sample has lost 3% of its initial weight. Moreover, it was established that the  $\text{NaNO}_3$  initial degradation temperature, 400 °C, is lower than the decomposition temperature of the material, 450 °C, showing thermal stability [10]. On the other hand,  $\text{NaNO}_2$  degrades above 330 °C. In this way, the first isothermal process must be reduced to 300 °C, ensuring that there is no weight loss and avoiding thermal instability [11]. Finally,  $\text{KNO}_3$  loses 0.044% of its weight at 180 °C, presenting stability [12]. These studies show the suitability of using  $\text{NaNO}_3$ ,  $\text{NaNO}_2$ , and  $\text{KNO}_3$  as thermal storage media due to their thermal stability. Nonetheless, it has been determined that eutectic mixtures of them are more promising for TES, as shown in [12].

Most of the current literature on inorganic salts as PCMs pays particular attention to binary or ternary mixtures because they provide advantages such as low costs, low vapor pressures, and high thermal stability [69]. In this way, it is essential to note the difference between eutectic and non-eutectic mixtures. Eutectic mixtures allow lower melting temperatures than the pure components, and at the same time, there is no segregation during the melting process [12]. On the other hand, although non-eutectic mixtures present segregation, they provide a higher range of temperature of phase change. Hence, mixtures of  $\text{NaNO}_3$ ,  $\text{NaNO}_2$ , and  $\text{KNO}_3$  have been identified as non-eutectic mixtures [7,51–53]. Nonetheless, further study is required due to the discrepancies. There is a contradiction in the previous analyzes carried out by different researchers; some determine that this combination is eutectic, and others determine that this system is of the continuous solid solution type [6].

Many studies have been focused on the use of nitrate salts as phase change materials. It has been demonstrated that the use of nitrate salts as PCMs have several applications such as small housing solar plants, water heating systems, solar cookers, and solar dryers [56–61]. To illustrate, a solar box cooker was fabricated with a ternary mixture of  $\text{NaNO}_3$ ,  $\text{NaNO}_2$ ,

and  $\text{KNO}_3$  as PCM. It was found that the PCM allows storing energy that can be used when solar radiation is absent. To be specific, approximately 108% higher was the load cooking time when using the PCM [58–65]. Moreover, a solar organic Rankine cycle plant was tested with the use of the non-eutectic mixture of  $\text{NaNO}_3$ ,  $\text{NaNO}_2$ , and  $\text{KNO}_3$  as the thermal storage system in a solar plant of 100 KWh [66,67]. Additionally, Prieto and Cabeza (2019) have used a cascade arrangement with different salts as PCMs including  $\text{NaNO}_3$  that allowed a lower cost and higher energy storage in solar power plants [66].

In the same token, concentrated solar power plants take advantage of the large thermal stability range of nitrate salts and use them as thermal storage systems [68]. In this sense, several studies have focused their attention on analyzing the thermal and chemical properties of these salts. Particularly, the effect of nitrogen and oxygen atmospheres on the performance of Solar Salt, the mixture of  $\text{NaNO}_3$  and  $\text{KNO}_3$ , and Hitec a ternary mixture of 53 wt %  $\text{KNO}_3$ , 7 wt %,  $\text{NaNO}_3$ , and 40 wt %  $\text{NaNO}_2$  was determined [24]. The former was stable under the mentioned atmospheres [67]. Nonetheless, Hitec presents the disadvantage that  $\text{NaNO}_2$  oxidizes under the presence of oxygen. Hence, it was established that inert atmosphere is required above 300 °C with nitrogen as an inert gas [70,71].

In this context, this research work determines the thermo-physical properties of nitrate salts ( $\text{NaNO}_3$ ,  $\text{NaNO}_2$ , and  $\text{KNO}_3$ ) and their binary and ternary combinations due to the discrepancy and errors associated with different experimental setups conducted in different studies. In this sense, this study tries to overcome the limitations in previous literature. Specifically, the properties of different salt mixtures are evaluated under the same methodological conditions. Based on this, nitrates as PMC were characterized through Fourier-transform infrared spectroscopy (FT-IR), differential scanning calorimetry (DSC), thermogravimetric analysis (TGA), and scanning electron microscopy (SEM) to establish their feasibility as PCMs for renewable energy storage applications.

## 2. Materials and Equipment

This section presents the selected materials and techniques used to evaluate the thermal, chemical, and morphological properties of three nitrate salts: sodium nitrate ( $\text{NaNO}_3$ ), potassium nitrate ( $\text{KNO}_3$ ), and sodium nitrite ( $\text{NaNO}_2$ ). The characterization was developed for the pure components and various combinations in different percentages by mass. For this research, the materials used were  $\text{KNO}_3$  of LOBA Chemie with 99% purity [73],  $\text{NaNO}_2$  of LOBA Chemie with 99% purity [74] and  $\text{NaNO}_3$  of LOBA Chemie with 99% of purity [75].

The following assay techniques were used: FTIR, to identify the material used; DSC, to find the enthalpy of phase change and specific heat; THM, as a complementary method to DSC to test the sample in a larger volume; TGA, to establish the thermal stability of the compound; and finally SEM, to verify the morphological characteristics of the sample after the heating process.

### 2.1. Materials

The selected granulated materials are  $\text{KNO}_3$ ,  $\text{NaNO}_3$ , and  $\text{NaNO}_2$ , which will be arranged in binary and ternary mixtures. To define these combinations, the phase diagram was considered, which shows the thermal behavior of the mixtures. Table 1 shows the name established for each compound, the percentage by mass of each combination, and the performed tests. Particularly, for binary compounds, the work developed by Berg [6] was consulted, which presents the binary phase diagram between  $\text{NaNO}_2$  and  $\text{NaNO}_3$ , considering the results of DSC tests and Raman spectroscopy. For the selection of the percentages of the binary compound mixture, the eutectic affinity of the materials involved and the need to consider a certain operating temperature for energy storage were considered. Additionally, the combination of  $\text{NaNO}_3$  and  $\text{KNO}_3$  in percentages of 60 and 40, respectively, was taken as a reference. This mixture is known as “Solar Salt” and has been extensively investigated.

Table 1. List of compounds.

Sample Number	Mass Percentage of the Mixtures			Assay Techniques				
	KNO <sub>3</sub> (wt %)	NaNO <sub>3</sub> (wt %)	NaNO <sub>2</sub> (wt %)	FTIR	DSC	THM	TGA	SEM
1	100	0	0	X	X		X	X
2	0	100	0	X	X		X	X
3	0	0	100	X	X		X	X
4	0	50	50		X	X		
5	53.5	46.5	0		X			
6	46.5	53.5	0		X			
7	43	57	0		X			
8	53	40	7		X			
9	40	53	7		X			
10	40	60	0		X	X		
11	53	7	40		X	X		

It is important to mention that the analyzed percentages were selected around the eutectic point of the mixture to verify whether the variations in the results found are significant. In Table 2, the thermal properties of the most common compounds found in the literature are shown. To verify that a PCM is suitable and meets the above selection criteria, it is important to determine its thermophysical properties. Conventional thermal characterization techniques include DSC analysis and differential thermal analysis (DTA). The high cost of the test equipment, its complexity, the lack of visualization of the phase change in the material, and the use of small samples of material cause the results found to vary because sometimes the behavior of a PCM depends on the quantity of it [33].

Table 2. Properties of the selected materials.

Property	1	2	3	4	5	6	7	9	11
Melting Temperature (°C)	333 [16]				221 [38]				
	336 [17]	308 [17]	279.8 [18]	220 [5]	222 [37]	222 [37]	137 [38]	220.9 [38]	142 [37]
	330 [16]	310 [5]	271.0 [36]		227 [39]		145 [37]	220 [37]	138 [38]
Melting Enthalpy (kJ/kg)	266 [18]	174 [17]			99–110 [38]				
	116 [17]	199 [18]	199.5 [17]	100.7 [5]	100 [37]	117 [14]	98.6 [38]	142.3 [38]	80 [37]
	266 [5]	172 [5]			108 [40]		97 [41]	142 [43]	17.2 [38]
Specific heat (kJ/kg K)	1.22 [5]	1.82 [5]			1.215 [38]				
	1.29 [42]	1.44 [42]	1.78 [42]	1.35 [5]	1.1 [41]	-	1.2 [38]	1.33 [38]	1.34 [38]

## 2.2. FTIR Analysis

The thickness of the sample must be appropriate for reducing the radiant power of the detector at the absorption frequencies used in the analysis. Before starting the procedure, preliminary preparation of the sample is important. In this case, due to the inherent hygroscopicity of molten salts, a drying pre-treatment is necessary. The procedure was verified by periodically measuring the variation in the weight of the samples every hour. The material containing the compound must be transparent to infrared radiation, such as potassium bromide (KBr), to ensure the measurement of absorption only of the sample. For solid samples, a small amount of pulverized KBr was mixed in an agate mortar and made into a pellet. The equipment used for the FTIR analysis was Perkin Elmer, Frontier model (Quito, Ecuador). The analysis was conducted in the range of 350–4000 cm<sup>-1</sup>. This test was carried out for the three pure salts, according to Table 1 compounds 1, 2, and 3.



### 2.3. Differential Scanning Calorimetry (DSC)

To perform these analyses, a Mettler Toledo differential scanning calorimeter was used. An amount of 5 to 7 mg of the samples were collocated in a pan. The heating rate was 10 °C/min [44]. For the analysis of the results, the thermal analysis system “STARe Evaluation Software” developed by the Mettler Toledo company (Quito, Ecuador) was employed.

According to Table 1, all compounds were tested by this method. The DSC analysis was developed in a Meter Toledo calorimeter, model: HP DSC 1, which consists of a chamber refrigeration equipment. Materials such as Indium and Zinc were used as reference elements to calibrate the equipment. According to [2], the phase change enthalpy was obtained according to Equation (1).

$$\Delta H = \int_{t_1}^{t_2} \phi dt = \int_{t_1}^{t_2} \frac{dH}{dt} dt \quad (1)$$

For the calculation of the  $C_p$ , Equation (1) is derived as a function of time. Where  $C_p$  is the specific heat of the sample,  $O$  is the heat flux;  $\beta_s$  is the heating rate ( $dT/dt$ ) and  $m$  is the mass of the compound.

$$C_p = \frac{dH/dt}{dT/dt} \frac{1}{m} = \frac{\phi}{\beta_s m} \quad (2)$$

### 2.4. Thermogravimetry Analysis (TGA)

A thermogravimetric analyzer SHIMADZU, TGA50 (Quito, Ecuador) was used. An amount of 2 to 4 mg of the samples were evaluated between 25 and 600 °C. A heating rate of 10 °C/min under an inert atmosphere of N<sub>2</sub> was used. This test has been carried out on compounds 1, 2, and 3 (see Table 1).

### 2.5. Scanning Electron Microscopy (SEM)

For this analysis, an electron microscope brand was used: TESCAN VEGA 3 SEM (Quito, Ecuador). Resolution in high vacuum mode ranges from 2 nm to 30 keV, and in low vacuum mode from 3.5 nm to 30 keV. The material is introduced into the sample holder together with a carbon filament to improve conductivity. As it is a non-conductive material, the surface must be metalized with gold under vacuum, applying a time of 60 s in the process. The parameters, acceleration voltage (HV), and working distance (WD) are important since they are related to the resolution and contrast of the image. This test has been carried out on compounds 1, 2, and 3 (see Table 1).

## 3. Results and Discussion

KNO<sub>3</sub>, NaNO<sub>2</sub>, and NaNO<sub>3</sub>, nitrate salts, and their binary and ternary mixtures were chemically and thermally characterized. Particularly, FTIR, DSC, TGA, and SEM analyses of the samples were conducted to obtain conclusive data about the workability of the nitrate salts as PCMs and avoid errors associated with the experimental setup.

### 3.1. FTIR Analysis

Through the FTIR analysis, it is possible to identify the functional groups of the molecules that make up the analyzed material, meaning that the composition of the sample could be known. The technique uses the infrared region of the electromagnetic spectrum.

This section shows the results of the characterization of sodium nitrate, potassium nitrate, and sodium nitrite according to the FTIR technique. Figure 1 shows several significant peaks such as the peak with the highest absorbance, 0.65, and occurs at a frequency of 1271.55 cm<sup>-1</sup>, corresponding to sodium nitrite. The analysis of the NaNO<sub>3</sub> compound in Figure 2 shows a peak with the highest absorbance, with a value of 4.89, at a frequency of 1370.02 cm<sup>-1</sup> corresponding to sodium nitrate. Likewise, the analysis of KNO<sub>3</sub> presents the peak with the highest absorbance of 0.85 with a frequency of 1384 cm<sup>-1</sup> in Figure 3. For the case of NaNO<sub>3</sub> and KNO<sub>3</sub>, the quantitative study of absorbance is around the band at 1385 cm<sup>-1</sup> (present in the IR spectra of the three compounds in KBr

medium). Therefore, it can be stated that there is no solid dissolution between KBr and the compounds analyzed [48].

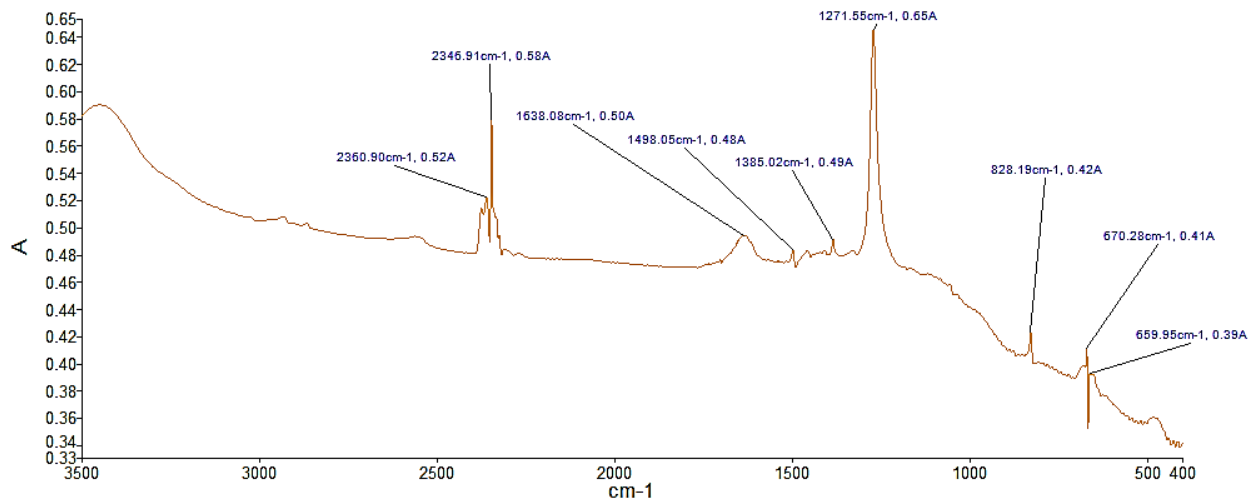


Figure 1. FTIR analysis of the NaNO<sub>2</sub> sample. A indicates absorbance.

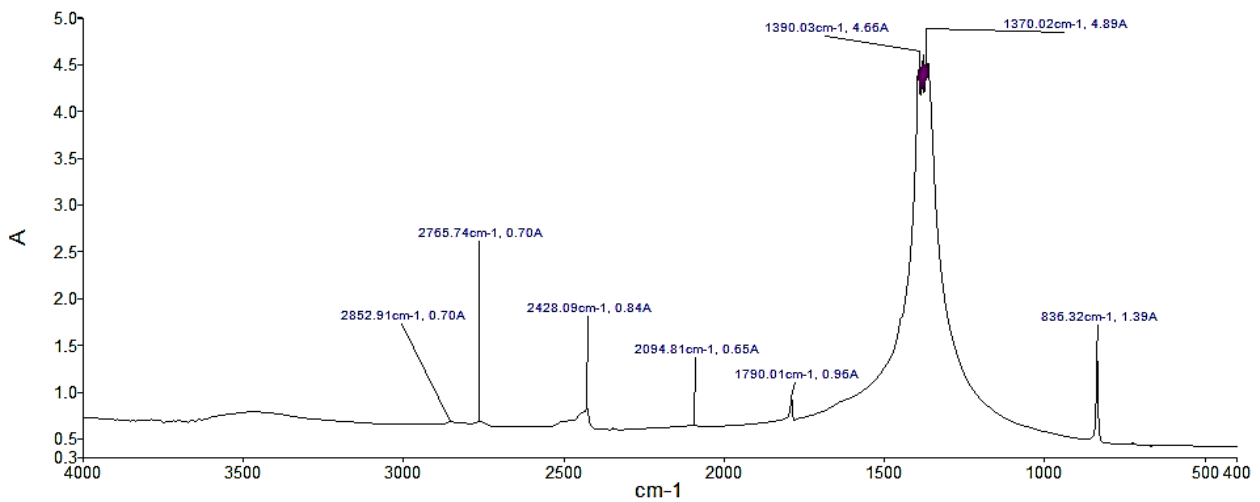


Figure 2. FTIR analysis of the NaNO<sub>3</sub> sample. A indicates absorbance.

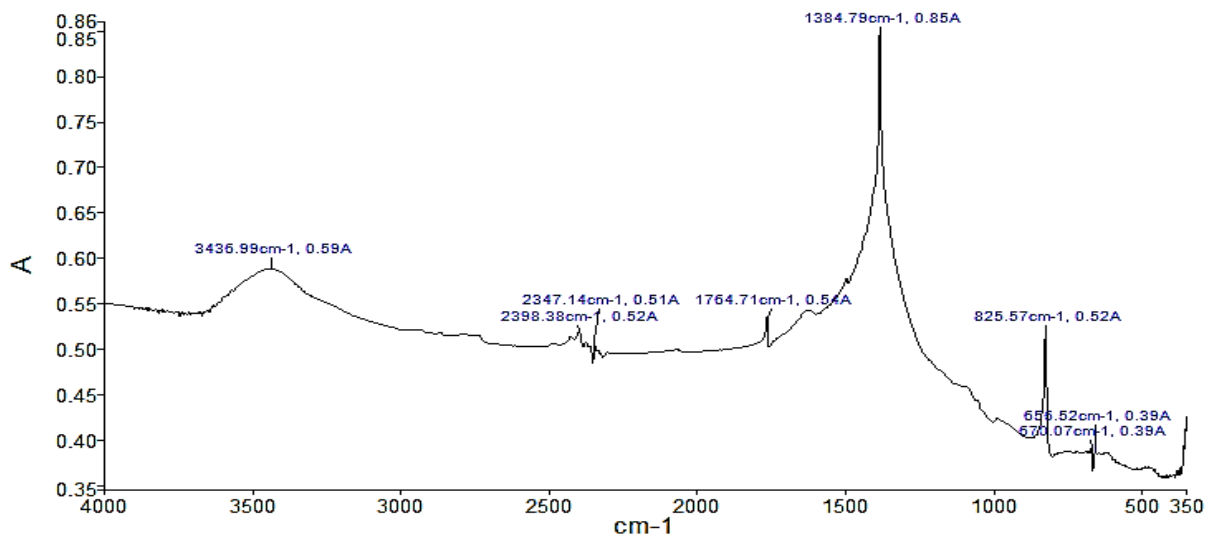


Figure 3. FTIR analysis of the KNO<sub>3</sub> sample. A indicates absorbance.

Specifically, the presence of the peak at  $1385\text{ cm}^{-1}$  is attributed to antisymmetric stretching of N–O vibration. In addition, in the presence of a peak at  $825\text{ cm}^{-1}$ , characteristics of the N–O out-of-plane bending, can be observed [26]. The abovementioned peaks confirm that the analyzed materials correspond to nitrate salts. Nonetheless, there was evidence for the presence of the O–H stretching around  $3440\text{ cm}^{-1}$ . Although the samples were dehydrated, this peak shows water absorption [54]. Moreover, in the case of the analysis of inorganic compounds, other characteristic values of absorbance and wave number can be observed. These values are captured due to the presence of impurities in the compound.

### 3.2. Differential Scanning Calorimetry (DSC)

The results of the DSC analysis allowed variables to be determined such as enthalpy of fusion, starting and ending temperatures of the endothermic process, and specific heat.

#### 3.2.1. Enthalpy of Fusion and Melting Temperature

Table 3 shows the evaluation of the compounds by DSC. Additionally, the DSC curves of compounds 1, 2, and 3 ( $\text{KNO}_3$ ,  $\text{NaNO}_3$ , and  $\text{NaNO}_2$ ) are presented in Figure 4.

Table 3. DSC results of the analyzed samples.

Sample Number	Mass Percentage of the Mixtures			DSC Parameters			
	$\text{KNO}_3$ (wt %)	$\text{NaNO}_3$ (wt %)	$\text{NaNO}_2$ (wt %)	T onset ( $^\circ\text{C}$ )	T end ( $^\circ\text{C}$ )	Fusion Temperature ( $^\circ\text{C}$ )	Enthalpy (J/g)
1	100	0	0	333.4	338.3	335.8	96.5
2	0	100	0	305.4	310.9	308.1	166.4
3	0	0	100	278.3	285.6	281.9	220.7
4	0	50	50	228.4	238.6	233.5	185.6
5	53.5	46.5	0	221.1	226.1	224.1	91.6
6	46.5	53.5	0	221.5	235.1	228.3	114.2
7	43	57	0	221.3	239.8	230.5	114.8
8	53	40	7	176.5	205.5	191	95.1
9	40	53	7	180.6	219.6	200.1	90.2
10	40	60	0	220.9	253.7	237.3	142.3
11	53	7	40	137.9	148.3	143.1	117.2

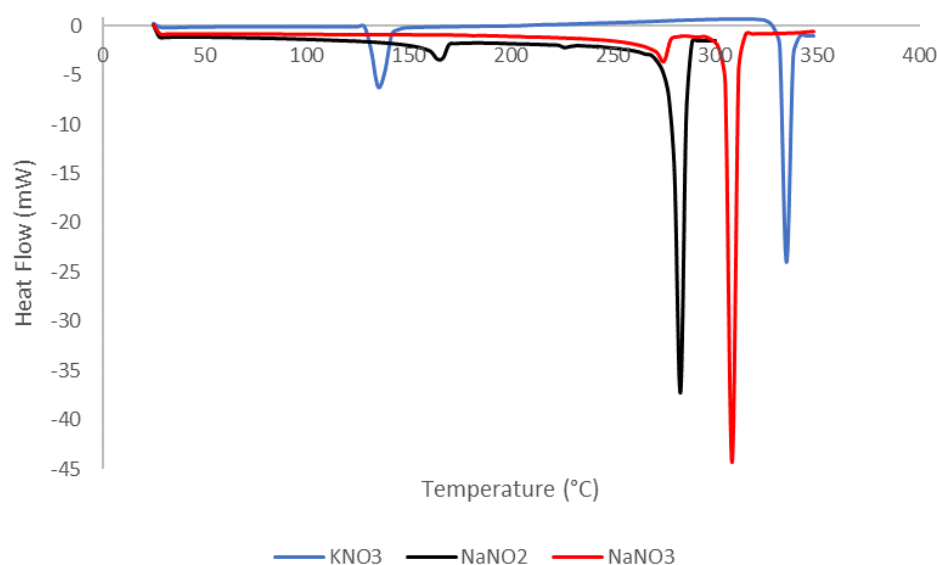


Figure 4. DSC curves of  $\text{KNO}_3$ ,  $\text{NaNO}_2$ , and  $\text{NaNO}_3$ .

$\text{KNO}_3$  compound exhibits two endothermic processes. The first corresponds to the solid–solid transition at a temperature of 130 to 135  $^\circ\text{C}$  with an enthalpy value of 47 kJ/kg.



As the temperature increases, another endothermic process is generated at 333 to 338 °C. This phase change corresponds to the solid to liquid (S–L) transition, since the starting temperature of the process and the melting point occur at the temperature peak with the highest heat flux, that is, at 334 °C, and the enthalpy of fusion reaches a value of 97 kJ/kg. The last value approximately doubles the value found during the solid to solid (S–S) transition process. The melting temperature around 333 °C matches an early study developed by Mohamed et al. [12]. Nevertheless, the heat of fusion was determined as 266 kJ/kg. This value is 85% higher than the value established in this study. Hence, this difference could be attributed to the impurities of the sample, as the FT-IR analysis showed.

Moreover, for NaNO<sub>3</sub>, the first endothermic process begins at a temperature of 271 °C and ends at 277 °C, presenting a tendency change at 276 °C. This is correlated to the S–S transition. In the same way, it was observed that the endothermic process produces an increase in the heat flux, generating a change in enthalpy of 107 kJ/kg. Subsequently, the increase in temperature generates the S–L transition process from 305 to 311 °C. Specifically, the phase change occurs at 306 °C with 166 kJ/kg as the value of the enthalpy of fusion. According to Li et al., the enthalpy of fusion and the melting temperature of the sodium nitrate are 178.6 kJ/kg and 306.4 °C, respectively [4]. Consequently, the findings of the current study are consistent with the abovementioned ones.

Furthermore, the analysis of NaNO<sub>2</sub> presents similar characteristics to Compound 2 (NaNO<sub>3</sub>) with the difference that the first endothermic process begins at 163 °C with a peak temperature at 165 °C. The process ends at 167 °C, and presents a change in enthalpy of 11 kJ/kg. The transition (S–L) occurs at 281 °C with an enthalpy of fusion of 221 kJ/kg. Kourkova et al. presented the thermal properties of NaNO<sub>2</sub> of 280 °C as the melting point and 221.7 kJ/kg as the latent heat of fusion [17]. Therefore, this study agrees with previous findings. It can be seen from figure x that NaNO<sub>3</sub> has a better performance than PCM due to its higher enthalpy of fusion compared with KNO<sub>3</sub> and NaNO<sub>2</sub>.

Compound 4, 50% of NaNO<sub>3</sub> and 50% of NaNO<sub>2</sub>, is a binary mixture that exhibits two transition processes, one from 163 to 167 °C. A peak has been obtained at the temperature of 165 °C which indicates the transition temperature S–S. Likewise, similar values are observed for the second endothermic process, from 228 to 239 °C. The phase change temperature is 231 °C and its phase change enthalpy is 186 kJ/kg.

In the same way, compound 5, 53.5% of KNO<sub>3</sub> and 46.5% of NaNO<sub>3</sub> (solar salt) present an endothermic process from 107 to 120 °C. The existence of a peak is observed at the temperature of 111 °C. The solid–solid transition corresponds to the first endothermic process. The second endothermic process presents a perceptible steeply sloping peak, whose heat flux is approximately eight times greater than the first process. This last process represents the change in state from solid to liquid, which begins at 221 °C and ends at 226 °C with a temperature peak at 223 °C. The analyzed mixture was determined to have a melting temperature of 223 °C, an enthalpy of melt of 92 kJ/kg. The present findings seem to be consistent with other research which found that the enthalpy of fusion of this mixture is 106 kJ/kg and the melting temperature is 223 °C [12]. The slight difference in the values of the enthalpy of fusion can be explained in part by the presence of impurities in the samples.

For the compound 6, which is 46.5% KNO<sub>3</sub> and 53.5% NaNO<sub>3</sub>, the test shows that as temperature increases, two endothermic processes occur, the first one from 107 to 118 °C. This process is quantified by its solid–solid transition enthalpy (S–S) of 23 kJ/kg. The second process was from 222 to 235 °C. In this process, the phase change (S–L) occurs, whose enthalpy of fusion is 114 kJ/kg. It is important to note that the peak value of this second process indicates the temperature at which the material changes from a solid to a liquid state; in this case at 225 °C. It is important to note that by switching the composition of the mixture, compounds 5 and 6, a higher enthalpy of fusion is achieved. This result is desired due to the increase in energy storage required in a PCM. In addition, compound 7 exhibits similar thermal properties to compound 6.

On the other hand, compounds 8, 9, and 11 are ternary mixtures. In Table 3, it is possible to see that compound 11 presented a better performance as PCM due to its higher enthalpy of fusion. From the evaluated compounds, although the selection of a PCM depends on the required temperature of phase change, it can be concluded that  $\text{NaNO}_2$  will have a better performance because of its higher energy storage capacity. Between the mixtures, the performance of 50% of  $\text{NaNO}_3$  and 50% of  $\text{NaNO}_2$  (compound 4), stands out compared to the other mixtures.

### 3.2.2. Specific Heat

It is important to mention that it is not possible to determine the specific heat during endothermic processes. Based on the DSC analysis results, this parameter was calculated by using methodology in [39], which relates the heat flow, the heating rate, and the mass of the compound. Table 4 shows the results of the specific heat for the solid and liquid state of the compounds, in the intervals where sensible heat exists.

**Table 4.** Specific heat of the evaluated compounds by DSC.

Compound	Mass (mg)	Molecular Weight (kg/mol)	Heat Flux S-S (mW)	Heat Flux S-L (mW)	Cps		Cpl	
					(J/kg K)	(J/mol K)	(J/kg K)	(J/mol K)
1	6.5	0.10	0.55	0.11	507.69	51.33	99.69	10.08
2	6.9	0.08	1.52	0.85	1321.74	112.32	739.13	62.81
3	5.7	0.07	1.76	1.52	1848.42	127.50	1600.00	110.37
4	6.4	0.08	1.74	1.98	1629.38	125.43	1855.31	142.82
5	6.4	0.09	1.28	1.51	1198.13	112.15	1419.38	132.86
6	7.0	0.09	1.80	1.44	1542.86	142.68	1234.29	114.14
7	6.7	0.09	1.33	1.14	1191.04	109.47	1020.90	93.83
8	7.0	0.09	3.03	8.88	2597.14	239.99	7611.43	703.34
9	7.0	0.09	1.75	1.93	1499.14	135.39	1656.00	149.55

In general, the compounds present specific heat values higher than 1000 J/kg·K either in a solid or liquid state, with exception of compounds 1 and 2 which show lower values. Compound 8 has the highest specific heat in solid and liquid states of 2597 J/kg K and 7611.43 J/kg K, respectively. Compound 3 has the second highest specific heat values of these compounds, which are 1848.42 and 1600.00 J/kg·K in the solid and liquid state, respectively. The lowest values were found to correspond to compound 1, which has values of 507.69 J/kg·K in solid-state and 739.13 J/kg·K in a liquid state. In the literature, it was found that the  $C_p$  in liquid state for compound 1 was 1190 J/kg·K, 1560 J/kg·K for compound 2, and 1350 for compound 5 [38]. Although these results differ from some published studies [42], the evidenced differences can be explained for the different methods used to determine the  $C_p$ . To be specific, the methodology applied in this study was numerical, and on the studies used for the comparison, there was an experimental  $C_p$  calculation based on a calorimeter.

### 3.3. Thermogravimetry Analysis (TGA)

One of the important parameters to select a PCM is to evaluate its operating temperature. Thermogravimetry analysis will help us determine the material's thermal stability; that is, it will find the variation in mass that the sample would experience as a function of the increase in temperature, which is caused by the fact that the system is not a hermetic system. This result made it possible to technically argue the feasibility of using PCM in low, medium, and high temperature thermal storage applications.

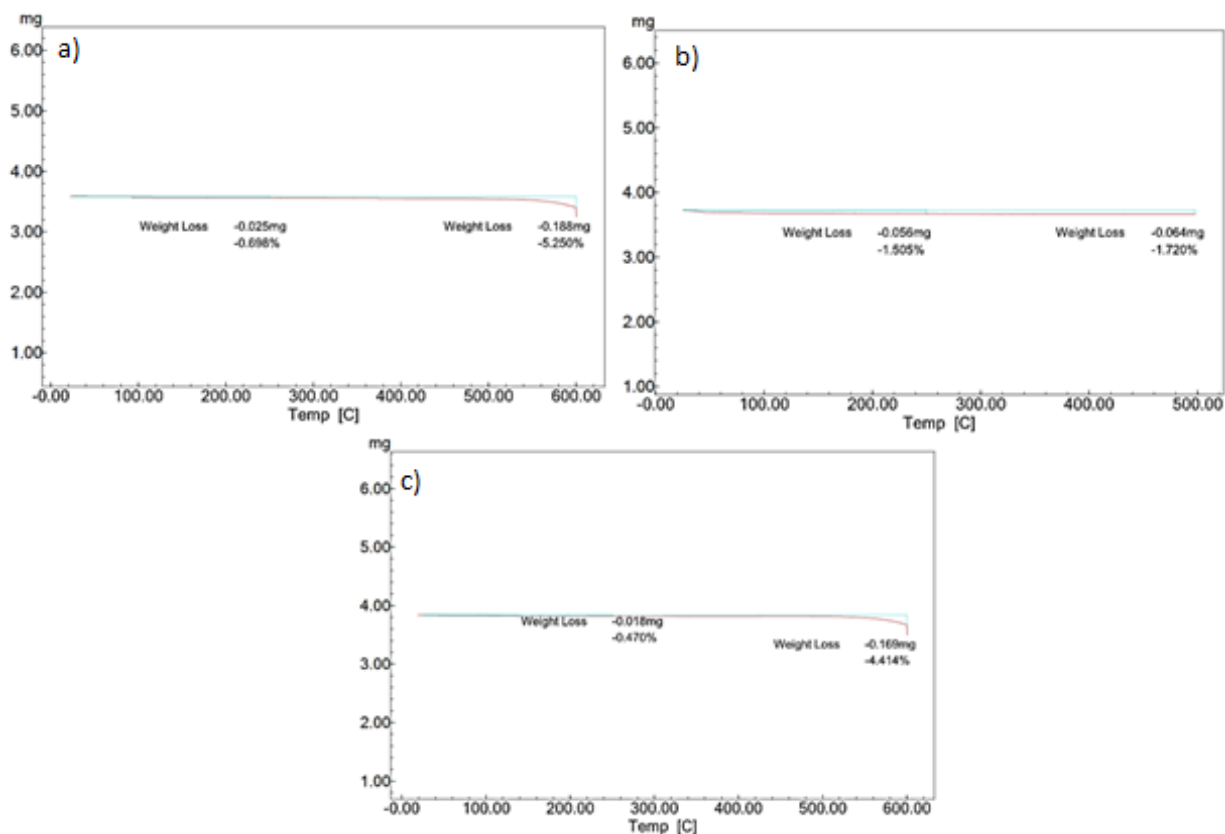
When exposed to high temperatures, alkali metal nitrate salts thermally decompose according to three different mechanisms [45]: (a) nitrite formation in the melt and oxygen release, (b) alkali metal oxide formation in the melt and nitrogen or nitrogen oxides release, and (c) vaporization of the nitrate salts.

Table 5 shows the results of weight variation in the samples analyzed by the TGA method. According to Table 5, point  $T_3$ , the maximum temperature or the stability limit where the sample has lost 3% of its initial weight [46,47], is exceeded during the test carried out on  $\text{NaNO}_3$ , even reaching 5.25% loss in weight at 600 °C. The same case is observed for  $\text{KNO}_3$ , which presents a loss of weight of 4.41% at 600 °C. It was found in the literature that the degradation temperature of  $\text{NaNO}_3$  sample starts at 400 °C [48]. Nonetheless, this value is below the temperature of decomposition of the material, 450 °C. On the other hand, to avoid the instability of  $\text{NaNO}_2$ , the first isothermal process was decreased to 300 °C [45].

**Table 5.** Results of the TGA analysis.

Parameters	Sample		
	(A) $\text{KNO}_3$	(B) $\text{NaNO}_3$	(C) $\text{NaNO}_2$
Initial weight of the sample (mg)	3.810	3.600	3.740
Weight loss (mg) at 250 °C	0.018	0.025	0.056
Percentage of weight loss (%) at 250 °C	0.47	0.70	1.51
Weight loss (mg) at 600 °C	0.169	0.188	0.064
Percentage of weight loss (%) a 600 °C	4.41	5.25	1.72

In Figure 5, the results obtained from the TGA analysis of the three compounds are shown. Two curves stand out; the first of them (cyan color), constitutes the reference of the initial mass of the sample, while the second (red color) shows the variation in this parameter as a function of the increase in temperature. The results obtained agree with the research carried out by [45]. The weight variation in the heating stage up to approximately 600 °C does not present a pronounced slope as observed in the case of bringing the material up to a temperature of 1000 °C. In this sense, these results show that the analyzed materials are thermally stable below 550 °C. Therefore, those materials can work stably as PCMs behind 600 °C.



**Figure 5.** TGA analysis of (a)  $\text{KNO}_3$ , (b)  $\text{NaNO}_3$ , and (c)  $\text{NaNO}_2$ .

### 3.4. Scanning Electron Microscopy (SEM)

This section presents the results obtained from the pure salts  $\text{KNO}_3$ ,  $\text{NaNO}_2$ , and  $\text{NaNO}_3$  using the scanning electron microscope (SEM). In Figure 6, four  $\text{KNO}_3$  images are shown with different image magnifications. The same acceleration voltage (HV) of 20.0 kV has been maintained for all observations. The working distance (WD) is in the range of 13.49 to 14.40 mm. With these parameters, the images with the best contrast were obtained. Grains can be seen with a size that varies from approximately 0.1 to 0.5 mm and no porosity or cracks are observed. Irregularly shaped particles are observed that are dispersed over the entire surface, agglomerating some particles with others.

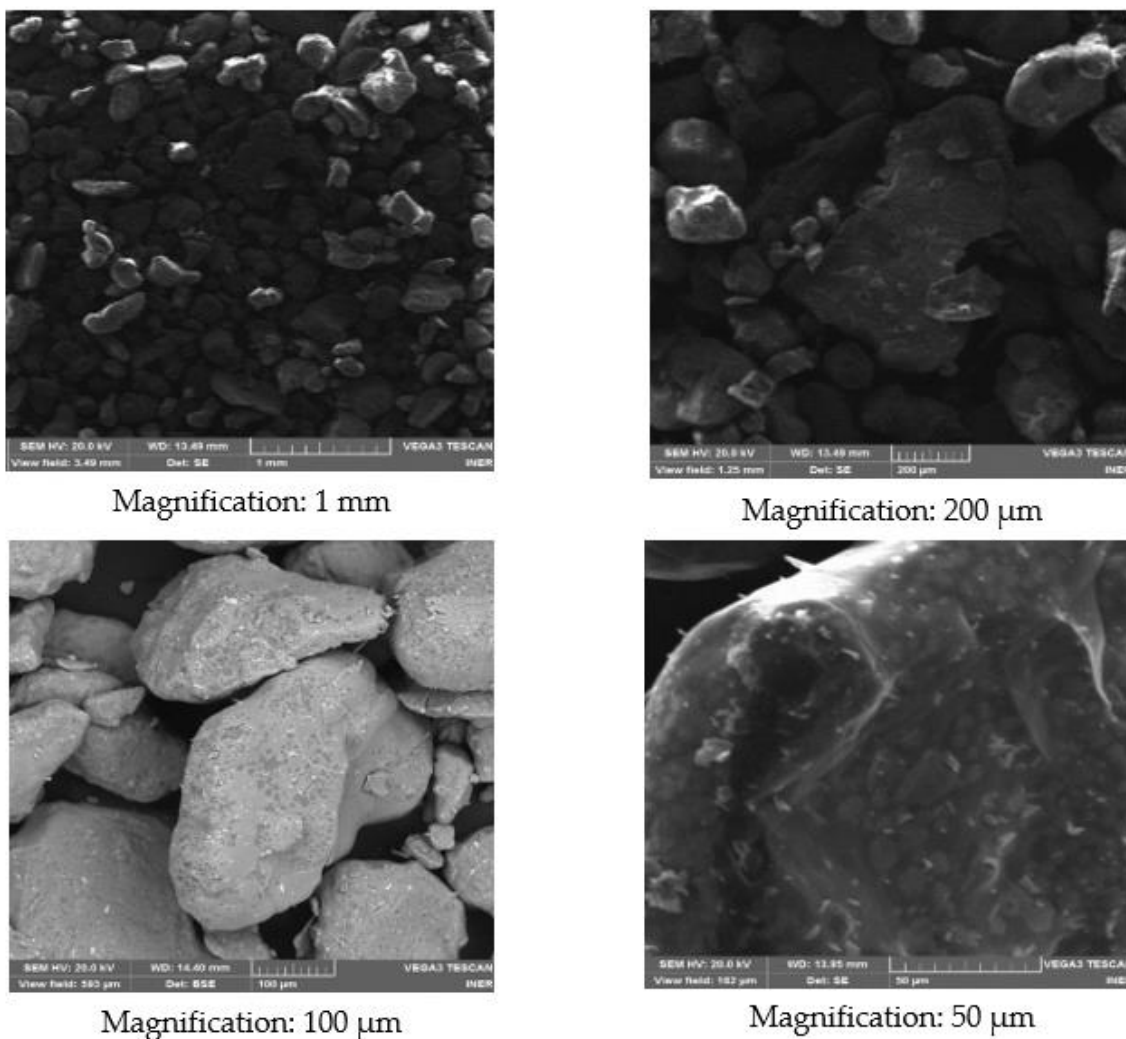


**Figure 6.** SEM images of the  $\text{KNO}_3$  sample.

Four images of  $\text{NaNO}_3$  are shown in Figure 7. An acceleration voltage (HV) of 5.0 kV has been maintained, except for the last image. The working distance (WD) is in the range of 9.73 to 13.95 mm. No porosity or cracks are observed, and 250 to 500  $\mu\text{m}$  of grains can be observed. Irregularly shaped particles are observed that are dispersed over the entire surface, agglomerating some particles with others. At higher magnifications of the microscope, flat surfaces are observed that will improve the reaction between particles.

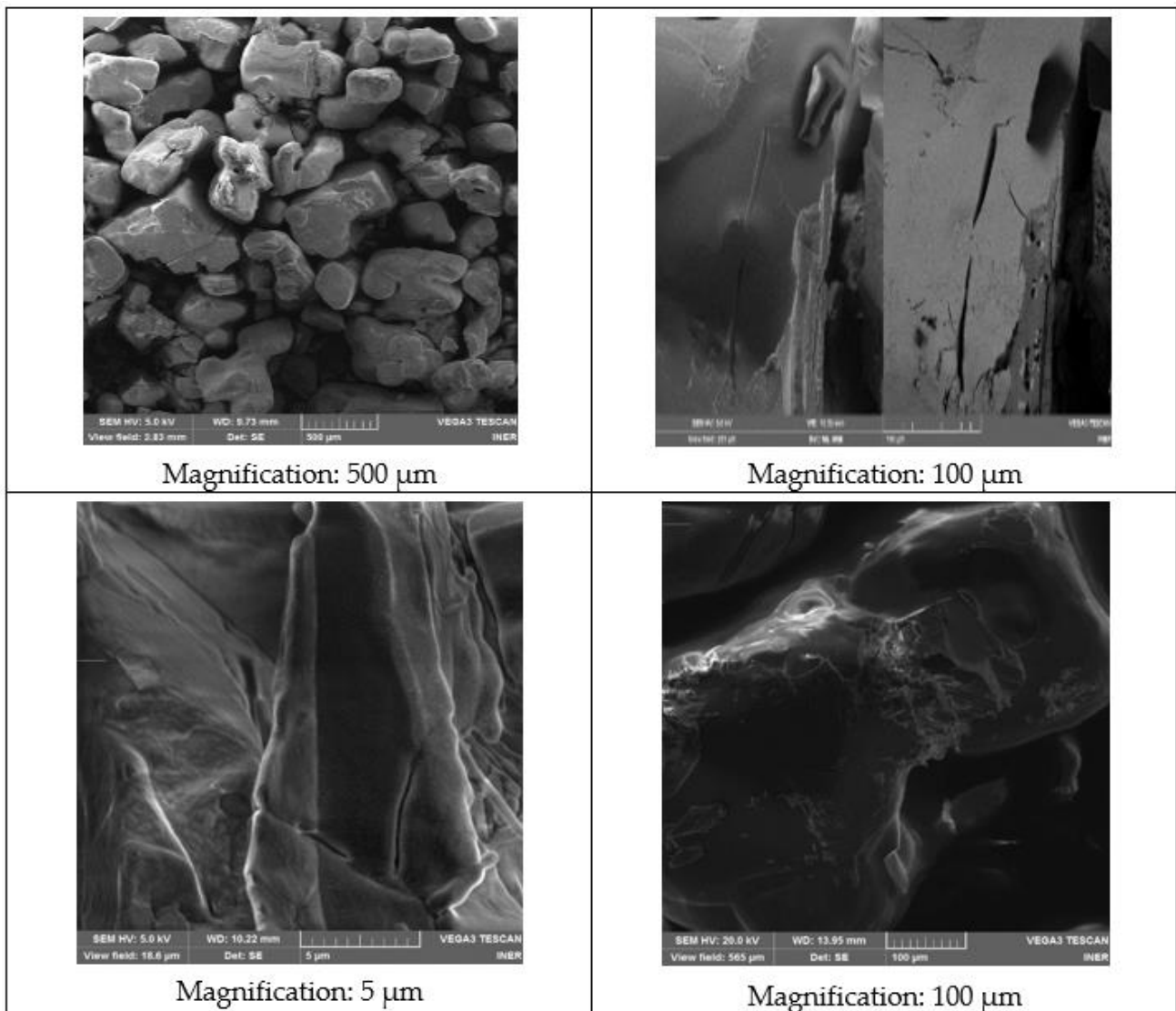


Figure 7. SEM images of the  $\text{NaNO}_3$  sample.

In Figure 8, four images of compound  $\text{NaNO}_2$  are shown. An acceleration voltage (HV) of 5.0 kV has been maintained. The working distance (WD) is around 10 mm. No porosity or cracks are observed and 250 to 500  $\mu\text{m}$  grains can be observed. Irregularly shaped particles are observed that are dispersed over the entire surface, agglomerating some particles with others.



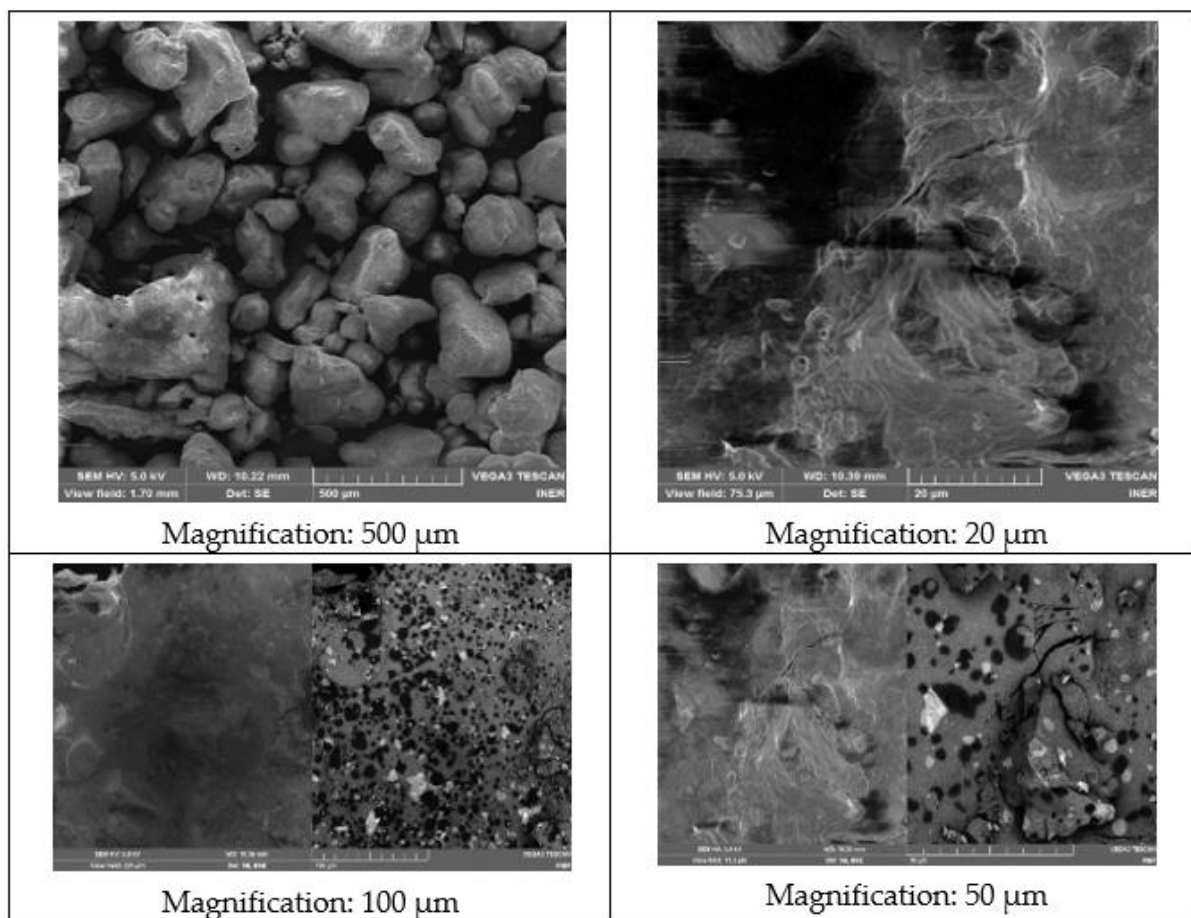


Figure 8. SEM images of the  $\text{NaNO}_2$  sample.

#### 4. Conclusions

In this study, the energy storage potential of nitrate salts and their mixtures for different purposes in energy systems from sustainable and renewable resources was evaluated. The FTIR analysis of the base salts confirmed the purity of the compounds. However, it was found that  $\text{KNO}_3$  presents water in its content. Moreover, from the TGA results, the  $\text{NaNO}_3$  and  $\text{KNO}_3$  materials exceed the limit temperature of degradation. This characteristic makes these materials not applicable for high-temperature energy storage applications.

On the other hand, emphasis is particularly placed on the greater enthalpy of fusion observed in sodium nitrite, 220.72 J/g. Nevertheless, it is important to consider not only this parameter but also the operating temperature of the system. Consequently, this PCM without mixtures will not be suitable for systems with operating ranges less than 278 °C.

In addition, the mixture of 50%  $\text{NaNO}_3$  and 50%  $\text{NaNO}_2$  presented an enthalpy of 185.6 J/g with a phase change start and end temperature of 228.4 and 238.6 °C, respectively. This result indicates that mixtures with sodium nitrite allow the thermal storage capacity of PCMs to increase. In this sense, it has been determined that this binary mixture will perform as a good PCM for medium-temperature storage systems.

In general, these materials are suitable for medium and high-temperature thermal energy storage systems due to their thermal and chemical stability and their high thermal storage capacity. In this sense, the results presented in this study can be used as an available source of thermal parameters of nitrites and nitrates as phase change materials obtained under a validated methodology. Therefore, these outcomes can be useful for the application of these PCMs in thermal energy storage systems.



**Author Contributions:** Conceptualization, M.A.O., J.M.-G. and A.C.-P.; methodology, M.A.O.; formal analysis, M.A.O., K.A., F.V.-A. and J.M.-G.; investigation, M.A.O., K.A., F.V.-A. and J.M.-G.; resources, M.A.O.; data curation, M.A.O.; writing—original draft preparation, M.A.O.; writing—review and editing, K.A., F.V.-A., A.C.-P. and J.M.-G.; supervision, J.M.-G.; project administration, J.M.-G.; funding acquisition, J.M.-G. All authors have read and agreed to the published version of the manuscript.

**Funding:** This research was funded by Secretaría de Educación Superior, Ciencia, Tecnología e Innovación (Senescyt), under national program of research funding “inérita” (programa nacional de financiamiento para investigación), project “Selección, caracterización y simulación de materiales de cambio de fase para confort térmico, refrigeración y almacenamiento de energía”. This research was funded by the project P121819, Parque de Energías Renovables founded by Universidad International SEK.

**Institutional Review Board Statement:** Not applicable.

**Informed Consent Statement:** Not applicable.

**Data Availability Statement:** Data presented in this study are openly available in <https://repositorio.uisek.edu.ec/>.

**Acknowledgments:** We would like to thank Diego Chulde, Danny Sinche, Michele Romero, Geovanna Villacreses and Paola Cuji from the Instituto de Investigación Geológico y Energético of Ecuador, for their help in the tests conducting.

**Conflicts of Interest:** The authors declare no conflict of interest.

## References

1. Kenisarin, M.M.; Mahkamov, K.; Costa, S.C.; Makhkamova, I. Melting and solidification of PCMs inside a spherical capsule: A critical review. *J. Energy Storage* **2020**, *27*, 101082. [[CrossRef](#)]
2. Kousksou, T.; Bruel, P.; Jamil, A.; El Rhafiki, T.; Zeraoui, Y. Energy storage: Applications and challenges. *Sol. Energy Mater. Sol. Cells* **2014**, *120*, 59–80. [[CrossRef](#)]
3. Pflieger, N.; Bauer, T.; Martin, C.; Eck, M.; Wörner, A. Thermal energy storage—Overview and specific in-sight into nitrate salts for sensible and latent heat storage. *Beilstein J. Nanotechnol.* **2015**, *6*, 1487–1497. [[CrossRef](#)] [[PubMed](#)]
4. Li, R.; Zhu, J.; Zhou, W.; Cheng, X.; Li, Y. Thermal properties of sodium nitrate-expanded vermiculite form-stable composite phase change materials. *Mater. Des.* **2016**, *104*, 190–196. [[CrossRef](#)]
5. Agyenim, F.; Hewitt, N.; Eames, P.; Smyth, M. A review of materials, heat transfer and phase change problem formulation for latent heat thermal energy storage systems (LHTESS). *Renew. Sustain. Energy Rev.* **2010**, *14*, 615–628. [[CrossRef](#)]
6. Pincemin, S.; Olives, R.; Py, X.; Christ, M. Highly conductive composites made of phase change materials and graphite for thermal storage. *Sol. Energy Mater. Sol. Cells* **2008**, *92*, 603–613. [[CrossRef](#)]
7. Berg, R.W.; Kerridge, D.H.; Larsen, P.H.  $\text{NaNO}_2 + \text{NaNO}_3$  Phase diagram: New data from DSC and raman spectroscopy. *J. Chem. Eng. Data* **2006**, *51*, 34–39. [[CrossRef](#)]
8. Andreu-cabedo, P. Mejora de las Propiedades Térmicas de Sal Solar Mediante Adición de Nanopartículas. Master’s Thesis, Universidad Jaume I, Castelló de la Plana, Spain, 2014.
9. Lu, W.; Liu, G.; Xiong, Z.; Wu, Z.; Zhang, G. An experimental investigation of composite phase change materials of ternary nitrate and expanded graphite for medium-temperature thermal energy storage. *Sol. Energy* **2020**, *195*, 573–580. [[CrossRef](#)]
10. Zhou, C.; Wu, S. Medium- and high-temperature latent heat thermal energy storage: Material database, system review, and corrosivity assessment. *Int. J. Energy Res.* **2018**, *43*, 621–661. [[CrossRef](#)]
11. Bakan, G.; Gerislioglu, B.; Dirisaglik, F.; Jurado, Z.; Sullivan, L.; Dana, A.; Lam, C.; Gokirmak, A.; Silva, H. Extracting the temperature distribution on a phase-change memory cell during crystallization. *J. Appl. Phys.* **2016**, *120*, 164504. [[CrossRef](#)]
12. Mohamed, S.A.; Al-Sulaiman, F.A.; Ibrahim, N.I.; Zahir, H.; Al-Ahmed, A.; Saidur, R.; Yılbaş, B.; Sahin, A.Z. A review on current status and challenges of inorganic phase change materials for thermal energy storage systems. *Renew. Sustain. Energy Rev.* **2017**, *70*, 1072–1089. [[CrossRef](#)]
13. Fernández, G.; Cabeza, L.F. Molten salt corrosion mechanisms of nitrate based thermal energy storage materials for concentrated solar power plants: A review. *Sol. Energy Mater. Sol. Cells* **2019**, *194*, 160–165. [[CrossRef](#)]
14. Cáceres, G.; Fullenkamp, K.; Montané, M.; Naplocha, K.; Dmitruk, A. Encapsulated nitrates phase change material selection for use as thermal storage and heat transfer materials at high temperature in concentrated solar power plants. *Energies* **2017**, *10*, 1318. [[CrossRef](#)]
15. Xu, G.; Leng, G.; Yang, C.; Qin, Y.; Wu, Y.; Chen, H.; Cong, L.; Ding, Y. Sodium nitrate—Diatomite composite materials for thermal energy storage. *Sol. Energy* **2017**, *146*, 494–502. [[CrossRef](#)]
16. Bauer, T.; Laing, D.; Tamme, R. Overview of PCMs for concentrated solar power in the temperature range 200 to 350 °C. *Adv. Sci. Technol.* **2011**, *74*, 272–277. [[CrossRef](#)]

17. Kourkova, L.; Svoboda, R.; Sadvovska, G.; Podzemna, V.; Kohutova, A. Heat capacity of NaNO<sub>2</sub>. *Thermochim. Acta* **2009**, *491*, 80–83. [[CrossRef](#)]
18. Zalba, B. Review on thermal energy storage with phase change: Materials, heat transfer analysis and applications. *Appl. Therm. Eng.* **2003**, *23*, 251–283. [[CrossRef](#)]
19. Chieruzzi, M.; Cerritelli, G.F.; Miliozzi, A.; Kenny, J.M.; Torre, L. Heat capacity of nanofluids for solar energy storage produced by dispersing oxide nanoparticles in nitrate salt mixture directly at high temperature. *Sol. Energy Mater. Sol. Cells* **2017**, *167*, 60–69. [[CrossRef](#)]
20. Ho, C.; Liu, Y.-C.; Ghalambaz, M.; Yan, W.-M. Forced convection heat transfer of Nano-Encapsulated Phase Change Material (NEPCM) suspension in a mini-channel heatsink. *Int. J. Heat Mass Transf.* **2020**, *155*, 119858. [[CrossRef](#)]
21. Eisapour, M.; Eisapour, A.H.; Hosseini, M.; Sardari, P.T. Exergy and energy analysis of wavy tubes photovoltaic-thermal systems using microencapsulated PCM nano-slurry coolant fluid. *Appl. Energy* **2020**, *266*, 114849. [[CrossRef](#)]
22. Hajjar, A.; Mehryan, S.; Ghalambaz, M. Time periodic natural convection heat transfer in a nano-encapsulated phase-change suspension. *Int. J. Mech. Sci.* **2020**, *166*, 105243. [[CrossRef](#)]
23. Talebizadehsardari, P.; Mahdi, J.M.; Mohammed, H.I.; Moghimi, M.A.; Eisapour, A.H.; Ghalambaz, M. Consecutive charging and discharging of a PCM-based plate heat exchanger with zigzag configuration. *Appl. Therm. Eng.* **2021**, *193*, 116970. [[CrossRef](#)]
24. Ho, M.X.; Pan, C. Optimal concentration of alumina nanoparticles in molten Hitec salt to maximize its specific heat capacity. *Int. J. Heat Mass Transf.* **2014**, *70*, 174–184. [[CrossRef](#)]
25. Hu, Y.; He, Y.; Zhang, Z.; Wen, D. Enhanced heat capacity of binary nitrate eutectic salt-silica nanofluid for solar energy storage. *Sol. Energy Mater. Sol. Cells* **2019**, *192*, 94–102. [[CrossRef](#)]
26. Myers, P.; Alam, T.E.; Kamal, R.; Goswami, D.; Stefanakos, E. Nitrate salts doped with CuO nanoparticles for thermal energy storage with improved heat transfer. *Appl. Energy* **2016**, *165*, 225–233. [[CrossRef](#)]
27. Ruiz-Cabañas, F.J.; Prieto, C.; Osuna, R.; Medina, V.; Fernandez, A.I.; Cabeza, L.F. Corrosion testing device for in-situ corrosion characterization in operational molten salts storage tanks: A516 Gr70 carbon steel performance under molten salts exposure. *Sol. Energy Mater. Sol. Cells* **2016**, *157*, 383–392. [[CrossRef](#)]
28. Riazi, H.; Mesgari, S.; Ahmed, N.A.; Taylor, R.A. The effect of nanoparticle morphology on the specific heat of nanosalts. *Int. J. Heat Mass Transf.* **2016**, *94*, 254–261. [[CrossRef](#)]
29. Grosu, Y.; Udayashankar, N.; Bondarchuk, O.; González-Fernández, L.; Faik, A. Unexpected effect of nanoparticles doping on the corrosivity of molten nitrate salt for thermal energy storage. *Sol. Energy Mater. Sol. Cells* **2018**, *178*, 91–97. [[CrossRef](#)]
30. Arthur, O.; Karim, M. An investigation into the thermophysical and rheological properties of nanofluids for solar thermal applications. *Renew. Sustain. Energy Rev.* **2016**, *55*, 739–755. [[CrossRef](#)]
31. Ahmed, S.F.; Khalid, M.; Rashmi, W.; Chan, A.; Shahbaz, K. Recent progress in solar thermal energy storage using nanomaterials. *Renew. Sustain. Energy Rev.* **2017**, *67*, 450–460. [[CrossRef](#)]
32. Fernández, A.; Galleguillos, H.; Fuentealba, E.; Perez-Trujillo, F.J. Corrosion of stainless steels and low-Cr steel in molten Ca(NO<sub>3</sub>)<sub>2</sub>-NaNO<sub>3</sub>-KNO<sub>3</sub> eutectic salt for direct energy storage in CSP plants. *Sol. Energy Mater. Sol. Cells* **2015**, *141*, 7–13. [[CrossRef](#)]
33. Yinping, Z.; Yi, J.; Yi, J. A simple method, the T-history method, of determining the heat of fusion, specific heat and thermal conductivity of phase-change materials. *Meas. Sci. Technol.* **1999**, *10*, 201–205. [[CrossRef](#)]
34. Solar, P.; Gmbh, I. *Survey of Thermal Storage for Parabolic Trough Power Plants Period of Performance: Survey of Thermal Storage for Parabolic Trough Power Plants Period of Performance*; NREL: Golden, CO, USA, 2000.
35. Graeter, F.; Rheinlander, J. *Thermische Energiespeicherung mit Phasenwechsel im Bereich von 150 bis 400 °C*; ZSW: Stuttgart, Germany, 2001; pp. 65–75.
36. Delise, T.; Tizzoni, A.C.; Votyakov, E.; Turchetti, L.; Corsaro, N.; Sau, S.; Licocchia, S. Modeling the total ternary phase diagram of NaNO<sub>3</sub>-KNO<sub>3</sub>-NaNO<sub>2</sub> using the binary subsystems data. *Int. J. Thermophys.* **2019**, *41*, 1. [[CrossRef](#)]
37. Kenisarin, M.M. High-temperature phase change materials for thermal energy storage. *Renew. Sustain. Energy Rev.* **2010**, *14*, 955–970. [[CrossRef](#)]
38. Gaona, D.; Urresta, E.; Marínez, J.; Guerrón, G. Medium temperature phase change materials thermal characterization by the T-history method and differential scanning calorimetry. *Exp. Heat Transf.* **2017**, *30*, 463–474. [[CrossRef](#)]
39. Cordaro, J.G.; Kruiuzenga, A.M.; Altmaier, R.; Sampson, M.; Nissen, A. Thermodynamic properties of mol-ten nitrate salts. *Mater. Sci.* **2011**, *1*, 925.
40. Janz, G.J.; Truong, G.N. Melting and premelting properties of the potassium nitrate-sodium nitrite-sodium nitrate eutectic system. *J. Chem. Eng. Data* **1983**, *28*, 201–202. [[CrossRef](#)]
41. Janz, G.J.; Allen, C.B.; Bansal, N.P.; Murphy, R.M.; Tomkins, R.P.T. *Physical Properties Data Compilations Relevant to Energy Storage. II. Molten Salts: Data on Single and Multi-Component Salt Systems*; U.S. Department of Energy Office of Scientific and Technical Information: Washington, DC, USA, 1979.
42. Kawakami, M.; Suzuki, K.; Yokoyama, S.; Takenaka, T. Heat capacity measurement of molten NaNO<sub>3</sub>-NaNO<sub>2</sub>-KNO<sub>3</sub> by drop calorimetry. In *Proceedings of the VII International Conference on Molten Slags Fluxes and Salts*; The South African Institute of Mining and Metallurgy: Johannesburg, South Africa, 2004; pp. 201–208.
43. Wagner, M.; Widmann, G. *Thermal Analysis in Practice*; Mettler-Toledo: Columbus, OH, USA, 2009.

44. Gimenez, P.; Fereres, S. Effect of heating rates and composition on the thermal decomposition of nitrate based molten salts. *Energy Procedia* **2015**, *69*, 654–662. [[CrossRef](#)]
45. Bauer, T.; Breidenbach, N.; Eck, M. Overview of molten salt storage systems and material development for solar thermal power plants. In Proceedings of the World Renewable Energy Forum 2012, Denver, CO, USA, 13–19 May 2012; pp. 1–8.
46. Raade, J.W.; Padowitz, D. Development of molten salt heat transfer fluid with low melting point and high thermal stability. *J. Sol. Energy Eng.* **2011**, *133*, 031013. [[CrossRef](#)]
47. Hoshino, Y.; Utsunomiya, T.; Abe, O. Thermal decomposition of sodium nitrate and the effects of several oxides on the decomposition. *Bull. Chem. Soc. Jpn.* **1981**, *54*, 1385–1391. [[CrossRef](#)]
48. Martínez, S.; Acción, F.; Puertas, F. Characterization of alkali-metal and alkaline-earth nitrates by vibrational spectroscopy. *Mater. Constr.* **1992**, *42*, 25–36. [[CrossRef](#)]
49. Berg, R.W.; Kerridge, D.H. The NaNO<sub>3</sub>/KNO<sub>3</sub> system: The position of the solidus and sub-solidus. *Dalton Trans.* **2004**, *15*, 2224–2229. [[CrossRef](#)] [[PubMed](#)]
50. Martin, C.; Bauer, T.; Müller-Steinhagen, H. An experimental study of a non-eutectic mixture of KNO<sub>3</sub> and NaNO<sub>3</sub> with a melting range for thermal energy storage. *Appl. Therm. Eng.* **2013**, *56*, 159–166. [[CrossRef](#)]
51. Zhang, X.; Tian, J.; Xu, K.; Gao, Y. Thermodynamic evaluation of phase equilibria in NaNO<sub>3</sub>-KNO<sub>3</sub> system. *J. Phase Equilibria Diffus.* **2003**, *24*, 441–446. [[CrossRef](#)]
52. Li, Y.; Guo, B.; Huang, G.; Shu, P.; Kiriki, H.; Kubo, S.; Ohno, K.; Kawai, T. Eutectic compound (KNO<sub>3</sub>/NaNO<sub>3</sub>: pcm) quasi-encapsulated into SiC-honeycomb for suppressing natural convection of melted PCM. *Int. J. Energy Res.* **2015**, *39*, 789–804. [[CrossRef](#)]
53. Romero-Sanchez, M.D.; Piticescu, R.R.; Motoc, A.M.; Popescu, L.M.C.; Tudor, A.I. Preparation of microencapsulated KNO<sub>3</sub> by solvothermal technology for thermal energy storage. *J. Therm. Anal. Calorim.* **2019**, *138*, 1979–1986. [[CrossRef](#)]
54. Mofijur, M.; Mahlia, T.M.I.; Silitonga, A.S.; Ong, H.C.; Silakhori, M.; Hasan, M.H.; Putra, N.; Rahman, S.M.A. Phase Change Materials (PCM) for solar energy usages and storage: An overview. *Energies* **2019**, *12*, 3167. [[CrossRef](#)]
55. Mahfuz, M.; Anisur, M.; Kibria, M.; Saidur, R.; Metselaar, H.S.C. Performance investigation of thermal energy storage system with Phase Change Material (PCM) for solar water heating application. *Int. Commun. Heat Mass Transf.* **2014**, *57*, 132–139. [[CrossRef](#)]
56. Pandey, A.K.; Hossain, M.; Tyagi, V.; Rahim, N.A.; Selvaraj, J.A.; Sari, A. Novel approaches and recent developments on potential applications of phase change materials in solar energy. *Renew. Sustain. Energy Rev.* **2018**, *82*, 281–323. [[CrossRef](#)]
57. Porteiro, J.; Míguez, J.L.; Crespo, B.; De Lara, J.; Pousada, J.M. On the behavior of different PCMs in a hot water storage tank against thermal demands. *Materials* **2016**, *9*, 213. [[CrossRef](#)] [[PubMed](#)]
58. Ling, D.; Mo, G.; Jiao, Q.; Wei, J.; Wang, X. Research on solar heating system with phase change thermal energy storage. *Energy Procedia* **2016**, *91*, 415–420. [[CrossRef](#)]
59. Benmoussa, F.; Benzaoui, A.; Benmoussa, H. Thermal behavior of latent thermal energy storage unit using two phase change materials: Effects of HTF inlet temperature. *Case Stud. Therm. Eng.* **2017**, *10*, 475–483. [[CrossRef](#)]
60. Zauner, C.; Hengstberger, F.; Mörzinger, B.; Hofmann, R.; Walter, H. Experimental characterization, and simulation of a hybrid sensible-latent heat storage. *Appl. Energy* **2017**, *189*, 506–519. [[CrossRef](#)]
61. Pelay, U.; Luo, L.; Fan, Y.; Stitou, D.; Rood, M. Thermal energy storage systems for concentrated solar power plants. *Renew. Sustain. Energy Rev.* **2017**, *79*, 82–100. [[CrossRef](#)]
62. Coccia, G.; Di Nicola, G.; Tomassetti, S.; Pierantozzi, M.; Chieruzzi, M.; Torre, L. Validación experimental de una cocina de caja solar de alta temperatura con una unidad de almacenamiento térmico a base de sal solar. *Energía Sol.* **2018**, *170*, 1016–1025. [[CrossRef](#)]
63. Coccia, G.; Di Nicola, G.; Pierantozzi, M.; Tomassetti, S.; Aquilanti, A. Design, manufacturing, and test of a high concentration ratio solar box cooker with multiple reflectors. *Sol. Energy* **2017**, *155*, 781–792. [[CrossRef](#)]
64. Costa, S.-C.; Mahkamov, K.; Kenisarin, M.; Lynn, K.; Halimic, E.; Mullen, D. Solar Salt Latent Heat Thermal Storage for a Small Solar Organic Rankine Cycle Plant. In Proceedings of the ASME 2018 12th International Conference on Energy Sustainability, Lake Buena Vista, FL, USA, 24–28 June 2018. [[CrossRef](#)]
65. Prieto, C.; Cabeza, L.F. Thermal energy storage (TES) with phase change materials (PCM) in solar power plants (CSP). Concept and plant performance. *Appl. Energy* **2019**, *254*, 113646. [[CrossRef](#)]
66. Ong, T.; Graham, E.; Will, G.; Steinberg, T.A. High-temperature phase change material (PCM) selection for concentrating solar power tower applications. *Adv. Sustain. Syst.* **2018**, *3*, 1800131. [[CrossRef](#)]
67. D’Aguanno, B.; Karthik, M.; Grace, A.N.; Floris, A. Thermostatic properties of nitrate molten salts and their solar and eutectic mixtures. *Sci. Rep.* **2018**, *8*, 10485. [[CrossRef](#)]
68. Villada, C.; Bonk, A.; Bauer, T.; Bolívar, F. High-temperature stability of nitrate/nitrite molten salt mixtures under different atmospheres. *Appl. Energy* **2018**, *226*, 107–115. [[CrossRef](#)]
69. Liu, M.; Tay, N.S.; Bell, S.; Belusko, M.; Jacob, R.; Will, G.; Saman, W.; Bruno, F. Review on concentrating solar power plants and new developments in high temperature thermal energy storage technologies. *Renew. Sustain. Energy Rev.* **2016**, *53*, 1411–1432. [[CrossRef](#)]
70. Prieto, C.; Miró, L.; Peiró, G.; Oró, E.; Gil, A.; Cabeza, L.F. Temperature distribution and heat losses in molten salts tanks for CSP plants. *Sol. Energy* **2016**, *135*, 518–526. [[CrossRef](#)]

71. Zhang, P.; Cheng, J.; Jin, Y.; An, X. Evaluation of thermal physical properties of molten nitrate salts with low melting temperature. *Sol. Energy Mater. Sol. Cells* **2018**, *176*, 36–41. [[CrossRef](#)]
72. Villada, C.; Jaramillo, F.; Castaño, J.G.; Echeverría, F.; Bolívar, F. Design and development of nitrate-nitrite based molten salts for concentrating solar power applications. *Sol. Energy* **2019**, *188*, 291–299. [[CrossRef](#)]
73. LOBA Chemie. Potassium-Nitrate. Available online: <https://www.lobachemie.com/Metallic-Salts-Metal-Salts-05400/POTASSIUM-NITRATE-CASNO-7757-79-1.aspx> (accessed on 29 July 2021).
74. LOBA Chemie. Sodium-Nitrite. Available online: <https://www.lobachemie.com/Inorganic-Salts-05954/SODIUM-NITRITE-CASNO-7632-00-0.aspx> (accessed on 29 July 2021).
75. LOBA Chemie. Sodium-Nitrate. Available online: <https://www.lobachemie.com/Inorganic-Salts-05949/SODIUM-NITRATE-CASNO-7631-99-4.aspx> (accessed on 29 July 2021).